European Rotorcraft Forum

IMPROVEMENT OF COMPUTATION EFFICIENCY FOR HELICOPTER ROTOR AERODYNAMIC ANALYSIS VIA ADAPTIVE WAVELET METHOD

Sanghyun Chae, nyugnas@pnu.edu, Pusan National University (Korea)
Sejong Oh, tazo@pnu.edu, Pusan National University (Korea)
Kwanjung Yee, daedalus@pnu.edu, Pusan National University (Korea)

Abstract

In helicopter aerodynamics, the accurate capture of tip vortices plays a key role in the prediction qualities of the helicopter performance. Huge amount of computational resources are usually required to avoid excessive numerical dissipation as well as to achieve proper vorticity conservation. For the application of rotor design, it is of crucial importance to present an efficient numerical method to circumvent excessive computational burden while keeping the necessary numerical accuracy. In this paper, the adaptive wavelet method is extended to enable efficient 3-D helicopter rotor analysis. The modifications for the improvement are: 1) temporal integration is executed only at the cells included in the adaptive dataset, 2) the wavelet decomposition is conducted intermittently, not on every iteration, 3) the additional cells are selected if neighbors are already included in the dataset, which helps to avoid spurious numerical oscillation. The capability of the modified wavelet method is demonstrated by the analysis of ONERA 7A hovering rotor. In this case, 37% of the elapsed time is saved on the background grid, while the accuracy of solution is almost retained.

1. INTRODUCTION

In the engineering design fields, the required computation resource and the numerical complication rapidly grow as computing hardware has been advanced, it is necessary to find an efficient calculation method when handling a realistic engineering problem. The design of helicopter rotor blades also needs tremendous iterative procedures to improve their performance, while the required prediction accuracy is increasing to that the use of CFD solvers becomes mandatory in the fields of aerodynamics and acoustics. For the practical design of helicopter rotor with CFD tools, the accuracy and efficiency of numerical simulation should be pursued simultaneously.

For the precise prediction of the performance Tip vortices of helicopter rotor are key matters. The flow fields of helicopter in hover and low speed forward flight are subject to strong influence of tip vortices emanating from the rotor blades because they resides close to the rotor and maintains their strength for several rotor revolutions. Each tip vortex and inboard sheet induces the strong downwash on the rotor disk; the accurate capture of these tip vortices plays a key role in the prediction of blade vortex interaction noise and the helicopter performance.

To achieve this goal, a huge amount of grid points and numerical scheme of higher order spatial accuracy are usually required. Though it is relatively easy to obtain adaptive grid system around moving tip vortices using the unstructured grid, the higher order scheme is rarely possible with this grid system. While the structured grid system can implement the high order scheme more easily than the unstructured grid system, grid adaptation is relatively difficult on structured grid system, which may result in inefficient use of grid points. This is particularly important in the helicopter rotor flow fields where only a small portion of computational domain undergoes meaningful gradients while other region essentially remains unchanged during the whole computational process.

It is a waste of the computational resources to use the fine grids in the whole domain for the vortex capturing, because the majority of the CFD data sets are in the smooth region in which the accurate solutions can be obtained with the relatively coarse grids. The dense grids are necessary only in the region of high gradient such as local flow fields around the vortices. Moreover, the time step is greatly limited according to the increment of the grid points.

For this reason, several types of adaptive methods have been implemented to improve the overall efficiency of the structured grid system. One of the representative techniques is the adaptive wavelet

method. The main feature of the adaptive wavelet method is to omit some mesh points from the given data set with the threshold value and improve the computational efficiency while retaining the solution accuracy. Currently, various numerical techniques based on the wavelet method have emerged for resolving the problems originated by the dense-grid system.

The adaptive wavelet method has been applied to CFD in different ways. Harten[1] presented an adaptive multiresolution scheme for computing the discontinuous solutions of hyperbolic PDEs. Holmström[2] proposed the algorithm that uses the interpolating wavelet transformation to organize an adaptive data set. Sjögreen[3] also used a multiresolution scheme based on the interpolating wavelet transformation to solve the compressible Euler equations. Vasilyev and Paolucci[4] extended the adaptive wavelet schemes to multidimensional partial differential equations. Kang et al.[5] suggested the modified wavelet method with the criterion of thresholding and stabilization coefficients. This method has merits of easy implementation and clear thresholding criteria, but has been applied to two dimensional application so far. Park et al.[6] extended the wavelet method of Kang et al.[5] to three dimension. Only second order of spatial accuracy was implemented, and elapsed time per iteration wasn't improved much, which is bad news for unsteady application. This adaptive wavelet method requires modifications for the extension of high order accuracy and the improvement of the calculation efficiency even in unsteady simulations.

The objective of this research is to achieve the efficient computation of aerodynamic analysis of three dimensional helicopter hovering rotor by the adaptive wavelet method with 3rd order accuracy of spatial scheme. For the precise capturing of rotor tip vortices, 3rd order MUSCL scheme is used in Roe's flux difference splitting and temporal integration is conducted by LU-SGS which has efficiency and robustness than alternative direction methods. The modifications of the adaptive wavelet method are suggested to reduce the elapsed time while keeping the numerical accuracy. The capability of modified wavelet method is demonstrated through the aerodynamic analysis of ONERA 7A[7] hovering rotor.

2. NUMERICAL METHODS

2.1. Implementation of Adaptive Wavelet Method on 3-D Euler Equations

For hovering rotor analysis, the three dimensional Euler equations are used as the governing equations. The three-dimensional Euler equations in a Cartesian reference frame rotating with angular velocity Ω of the rotor are written as Eq. (1).

(1)

$$\frac{\partial Q}{\partial t}+\frac{\partial E}{\partial x}+\frac{\partial F}{\partial y}+\frac{\partial G}{\partial z}=S$$

with $Q=\begin{bmatrix}\rho\\ \rho u\\ \rho v\\ \rho w\\ \rho e_t\end{bmatrix}$, $E=\begin{bmatrix}\rho u\\ \rho u^2+p\\ \rho uv\\ \rho uw\\ (\rho e_t+p)u\end{bmatrix}$, $F=\begin{bmatrix}\rho v\\ \rho vu\\ \rho v^2+p\\ \rho vw\\ (\rho e_t+p)v\end{bmatrix}$,

$G=\begin{bmatrix}\rho w\\ \rho wu\\ \rho wv\\ \rho w^2+p\\ (\rho e_t+p)w\end{bmatrix}$, $S=\begin{bmatrix}0\\ -\rho\Omega w\\ 0\\ \rho\Omega u\\ 0\end{bmatrix}$ and

$$e_t=\frac{p}{\gamma(\gamma-1)}+\frac{1}{2}(u^2+v^2+w^2)$$

In order to conduct the calculations with an arbitrary curvilinear grid system, these equations are transformed from the Cartesian coordinate system to the generalized coordinate with non-dimensionalization as rewritten as Eq. (2).

(2)

$$\frac{\partial \bar{Q}}{\partial \tau}+\frac{\partial \bar{E}}{\partial \xi}+\frac{\partial \bar{F}}{\partial \eta}+\frac{\partial \bar{G}}{\partial \zeta}=S$$

with $\bar{Q}=\frac{Q}{J}$, $\bar{E}=\frac{1}{J}[\xi_t Q+\xi_x E+\xi_y F+\xi_z G]$,

$\bar{F}=\frac{1}{J}[\eta_t Q+\eta_x E+\eta_y F+\eta_z G]$,

and $\bar{G}=\frac{1}{J}[\zeta_t Q+\zeta_x E+\zeta_y F+\zeta_z G]$

The adaptive wavelet method is implemented to CFD solver of three dimensional Euler equations. And the reference method of wavelet was chosen as the adaptive wavelet method suggested by Kang et al.[5]. The adaptive wavelet uses the interpolating wavelet transformation including decomposition and threshold to construct an adaptive dataset to a solution. This is, the cells in which the interpolated values have enough accuracy are excluded, the other cells included in the adaptive dataset. Then, fluxes are calculated only at the points within the adaptive dataset, which enhances the computational efficiency. Details of the reference wavelet method is

written in appendix.

2.2. Modification of Adaptive Wavelet Method

If the method is to be directly employed for 3-D application, there are several numerical issues to be solved. Park et al.[6] demonstrated the wavelet method on the aerodynamic analysis of ONERA M6 wing with 2nd order MUSCL and LU-SGS, insisted that reduced one third of calculation elapsed time. However, their method had limitation of 2nd order of spatial accuracy, and the elapsed time per iteration was not improved much; the acceleration was achieved mainly by fast convergence. In this paper, further modifications are devised for the more efficient adaptive wavelet method.

The previous adaptive method doesn't reduce elapsed time of the temporal integration step. Although flux evaluation is only conducted in the adaptive dataset and the residuals of excluded cells are interpolated on the spatial discretization step, temporal integration executes on the whole computational domain.

2.2.1. Reduction of temporal integration in LU-SGS

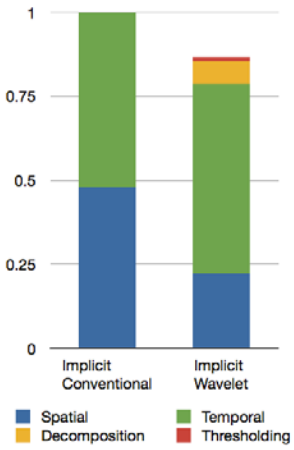

Fig. 1 Elapsed time comparison of each procedure (LU-SGS).

Implicit methods including LU-SGS require more calculation burden than that of explicit methods. Temporal integration(LU-SGS) routine takes almost half of the elapsed time for one iteration as shown in Fig. 1. If the adaptive wavelet method reduces elapsed time of spatial discretization to about half, this reduction enables 15% decrease of entire calculation time. The degradation of the efficiency is caused by the additional time of the wavelet decomposition and thresholding routines and the unchanged time of the temporal integration.

Therefore, a novel method is suggested to reduce the elapsed time of temporal integration by LU-SGS. The simplest way is that the temporal integration of LU-SGS is conducted at cells included in the adaptive dataset, after residual interpolation is omitted. In the adaptive dataset, the neighbor cell of the under-evaluating cell may be absent, and this may deteriorates the robust or the accuracy of solver. Thus, the nearest cell of the evaluating point should be moved to the neighbor of the evaluating cell as shown in Fig. 2. The use of this gathering of neighbor cells in LU-SGS may increase the error of the approximation on the diagonal matrix and deteriorate the accuracy or the convergence of the solution. However, there has been no difference on the solution accuracy and robustness between the conventional solver and the modified wavelet solver, practically.

After the temporal integration, the residuals on the excluded cells are interpolated.

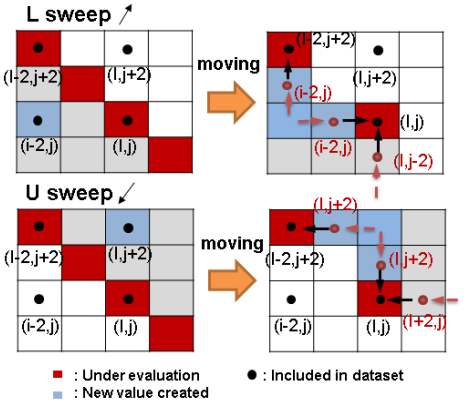

Fig. 2 Cell gathering in the adaptive dataset on LU-SGS.

2.2.2. Numerical Noise

In three dimensional extension of the adaptive wavelet, one serious issue is the appearance of numerical noise, which degenerates not only the quality of numerical solution but also the efficiency of adaptive wavelet.

In the present research, two possible reasons are considered for the occurrence of numerical noise. One is the scattered distribution of cells in the adaptive dataset, the other is frequent change of the adaptive dataset. Two remedies are implemented for the solution of each reason, respectively.

To relieve the scattered distribution of cells, some

cells can be added after the adaptive dataset construction. If one cell is neighboring to the cell which is already included in the dataset, some weight value(0.4) is given to the cell. If an excluded cell has the weight value more than 1, which means that it is neighboring more than 3 cells in the original dataset, the cell is added to the adaptive dataset as shown in Fig. 3. Although computation time is slightly increased due to added cells in the data set, it is possible to obtain more smooth numerical solution.

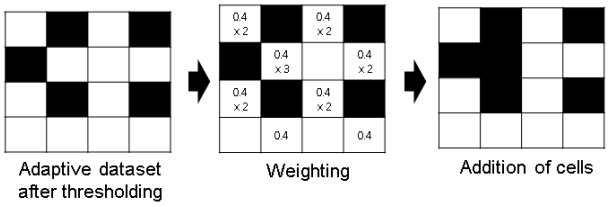

Fig. 3 Cell addition by weighting value

2.2.3. Intermittent wavelet decomposition

The other useful modification is the intermittent execution of the wavelet decomposition. At the decomposition process, the adaptive dataset is reconstructed, so execution of the decomposition at every iteration may occur the frequent change of adaptive dataset. To build the robust dataset, the decomposition is conducted once every 10 iterations.

3. RESULTS AND DISCUSSIONS

For the demonstration of the modified adaptive wavelet method, the aerodynamic performance of ONERA 7A rotor is calculated. It is a four-bladed rotor with an aspect ratio of 15 and consists of rotor airfoils of the OA2XX series with 13% and 9% airfoil thickness. For this test case, the hover condition with a collective pitch $\theta_{0.7} = 7.5^\circ$ giving the thrust coefficient $C_T = 0.068$ and a tip speed $M_{tip} = 0.6612$ was selected[7]. This validation test case should prove the capability of the modified adaptive wavelet method to predict the flow filed around a rotor accurately and efficiently.

In the application of the helicopter rotor analysis, the overset grid technique is mandatory for the structured grid system. Fig. 4 shows the schematic diagram of the grid system which consists of the background grid and the inner rotor grid. The overall perspective views of the background and rotor grid are presented in Fig.5. The number of each grid described in Table 1.

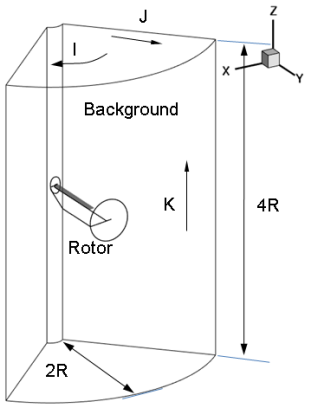

Fig. 4 Schematic diagram of grid system.

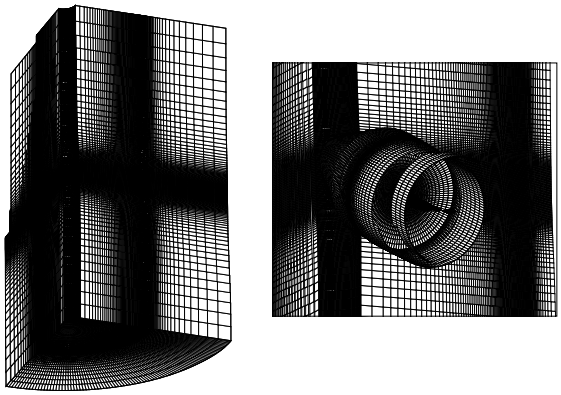

Fig. 5 Background periodic O-H mesh(left) and ONERA 7A rotor mesh(right).

Table 1 Number of each grid

	Number of grid
Background (O-H type)	91 × 134 × 161 =1,963,234 (i × j × k in Fig. 6)
Rotor (O-H type)	131 × 77 × 51 = 514,437 (chordwise × spanwise × normal)
On surface	131 × 58 = 7,598

For the calculation, Roe's flux difference splitting scheme with 3rd order Koren's limiter for spatial discretisation and LU-SGS for temporal integration was used. The boundary conditions are implemented as the slip wall condition on a rotor surface, zero normal flow condition on the hub boundary. A periodic conditions are used on upstream and downstream surfaces of the background for four-bladed rotor hovering. The outer-boundary values are specified by an approximate source-sink condition[8].

For the modified wavelet method, the interpolation error is set to $\varepsilon = 1 \times 10^{-5}$. The modified wavelet method was applied to the background grid. The majority of the background region is in the smooth region, rotor wakes occupy local flow field which should be included in the adaptive dataset. Thus, the capability of the modified wavelet method is prominently revealed on the background grid.

The comparisons of the convergence histories are shown in Fig. 6 and Fig. 7. The density residual dropped more than 4 orders of magnitude and it can be noted that the convergence trends between the conventional solver and the solver with the modified wavelet are similar in Fig. 6. Fig. 7 shows the thrust of both solvers converged above 4,000 iterations and the use of the adaptive wavelet has little effect on the convergence of thrust coefficient. The converged thrust coefficients of both solvers have a good agreement with experimental result.

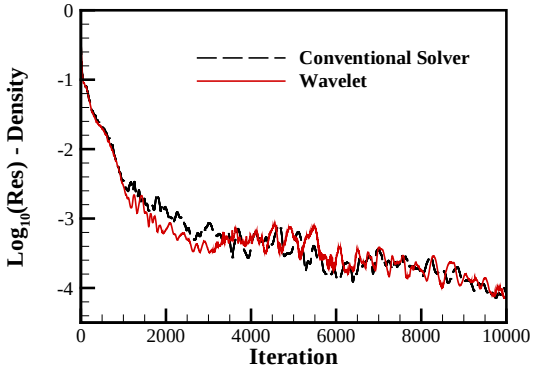

Fig. 6 Convergence history of density residual.

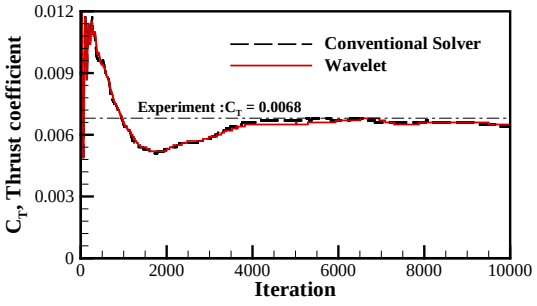

Fig. 7 Convergence history of thrust coefficient.

Table 2 Comparison of thrust coefficients

	Thrust coefficient (% difference ratio to experimental value)
Experiment	0.0068
Conventional	0.0064 (6%)
Wavelet	0.0065 (4%)

The improvement of the modified wavelet method is proved by the comparison of the elapsed time until 10,000 iterations in Table 3. The modified wavelet method saved 24% of the overall calculation time, although the overall elapsed time includes the calculation time of the inner rotor grid, the interpolation time between the background and the inner grid for the overset grid technique, and writing time of intermediate result files. This overall improvement can be changed by the environment and configuration of the solver. It is noted that the pure calculation elapsed time on the background grid was reduced to 63% by the modified adaptive wavelet method; 37% of the elapsed time was saved. While the adaptive dataset was constructed with 42% of number of the background grid, the modified LU-SGS which conducts at only included cell accelerates the improvement of efficiency as explained in Sec. 2.2.1. Fig. 8 shows the modification on LU-SGS decreases the elapsed time on temporal integration as much as time reduction on spatial discretization.

Table 3 Comparison of the calculation time.

	Elapsed time (sec.)	
	Background	Overall
Conventional	63168	95820
Wavelet	39931	72450
Saved time (% of $1 - \frac{\text{Wavelet}}{\text{Conventional}}$)	37%	24%

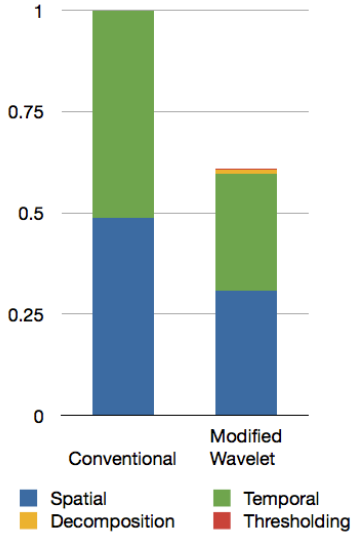

Fig. 8 Elapsed time comparison of modified wavelet method.

The accuracy of the modified adaptive wavelet method is shown through the comparison with the results of the conventional solver. Pressure distributions on the surfaces at 50%, 82.5%, 91.5% and 97.5% of ONERA 7A rotor span are presented in Fig. 9. The computational results are in good agreement with the experimental and EROS results[7]. The pressure distribution predicted by the modified wavelet solver has almost same with that of the conventional solver. Fig. 10 shows the comparison between the numerical results and the experimental data in terms of normal force coefficient $C_N M^2$. In the comparison of the normal force coefficient, the numerical results still agrees well with the experimental data and EROS results[7] and between the conventional solver and the wavelet solver. These comparisons support that the accuracy of the wavelet method is retained on the blade surface.

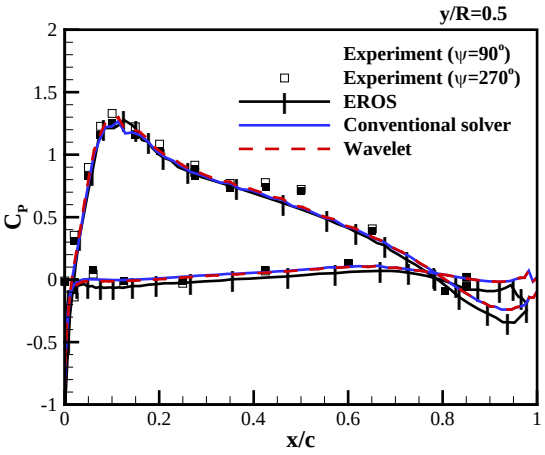

(a) y/R = 0.5

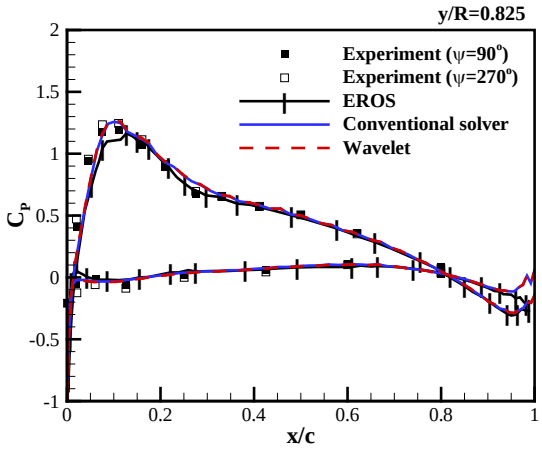

(b) y/R = 0.825

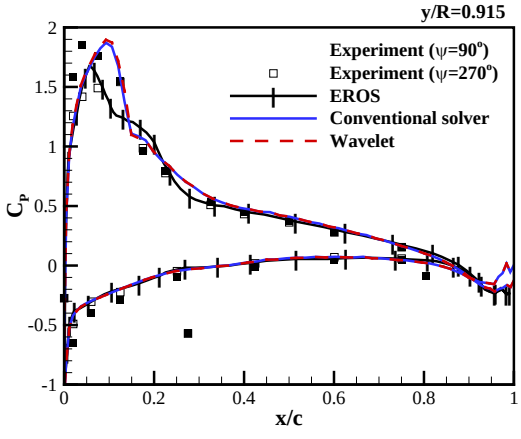

(c) y/R = 0.915

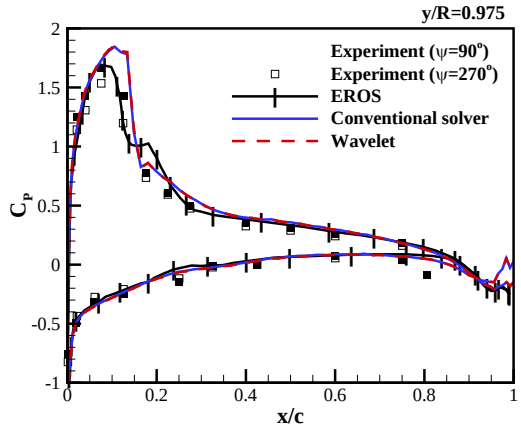

(d) y/R = 0.975

Fig. 9 Pressure distribution on the surface of ONERA 7A rotor.

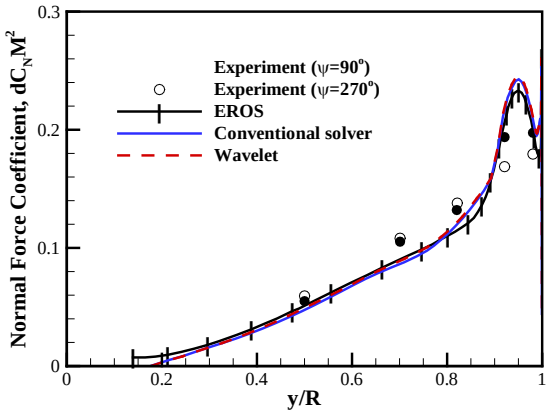

Fig. 10 Normal force coefficient distribution along the blade span.

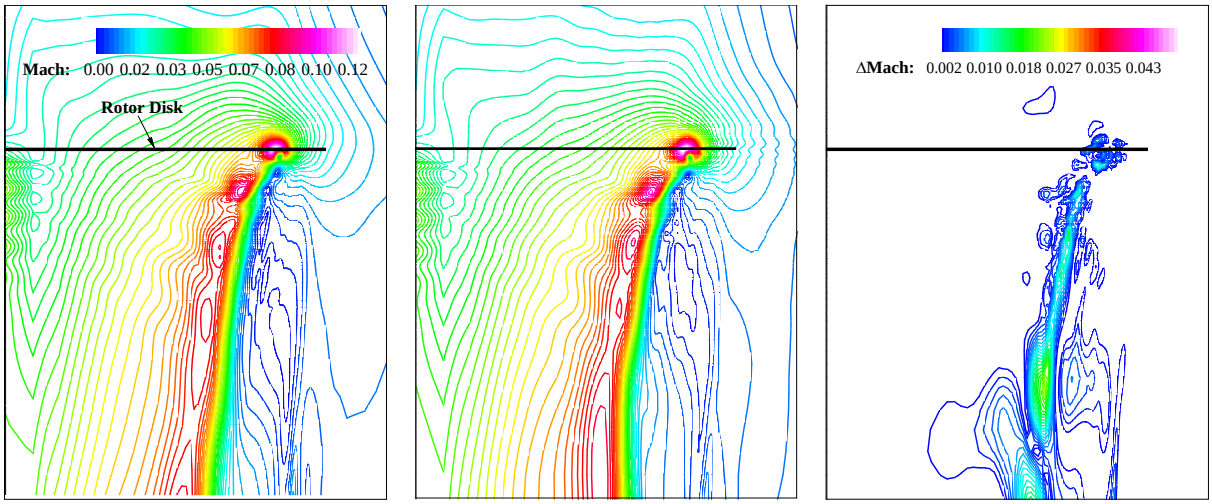

(a) Conventional solver (b) Wavelet (c) Difference

Fig. 11 Mach contour plot comparison at the azimuthal station of 60° behind the blade.

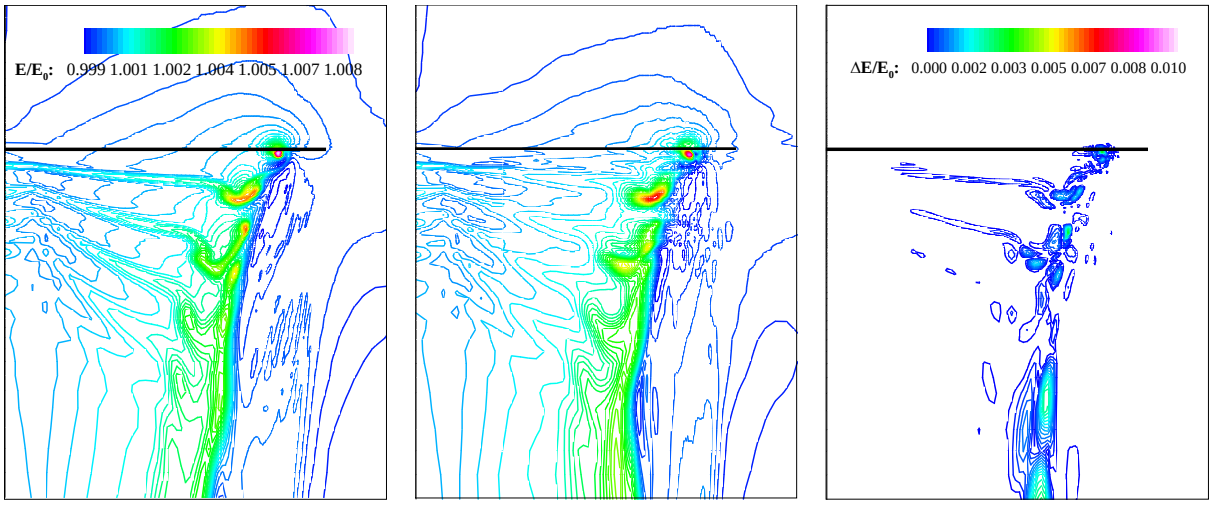

(a) Conventional solver (b) Wavelet (c) Difference

Fig. 12 Energy contour plot comparison at the azimuthal station of 60° behind the blade.

For the verification of the accuracy in the flow field, Mach contours and energy field contours are presented in Fig. 11 and Fig. 12, respectively. There are tiny differences between two solvers in the majority of the flow field. Around the stream line constructed by tip vortex, significant differences are generated locally. In Fig. 12, regions of energy changed by shed wakes have some differences between the conventional and the wavelet solver. It means the wavelet method doesn't include enough cells around the regions in which properties are changed abruptly.

Fig. 13 shows the isosurface of Q-criteria in the flowfield calculated by the conventional solver and the wavelet solver. The trajectories of tip vortex are similar between two solvers. However, the isosurfaces of the wavelet method becomes rough. It is caused by the coarse adaptive dataset as shown in Fig. 13 (b).

Quantitative measurements of the tip vortex trajectories are compared with experimental values and EROS results[7] in Fig. 14. The conventional solver and the wavelet solver are in good agreement

with the experimental and EROS results[7]. Although comparisons of flow field contours and the isosurfaces of Q-criteria reveal the difference between two solver and the large difference regions are focused around tip vortices, these errors don't cause a serious problem on accuracy. This is proved by the comparison results of pressure distribution and the wake trajectories between two solvers.

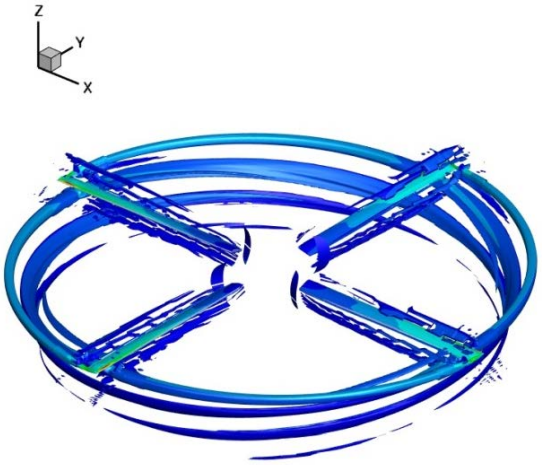

(a) Conventional Solver

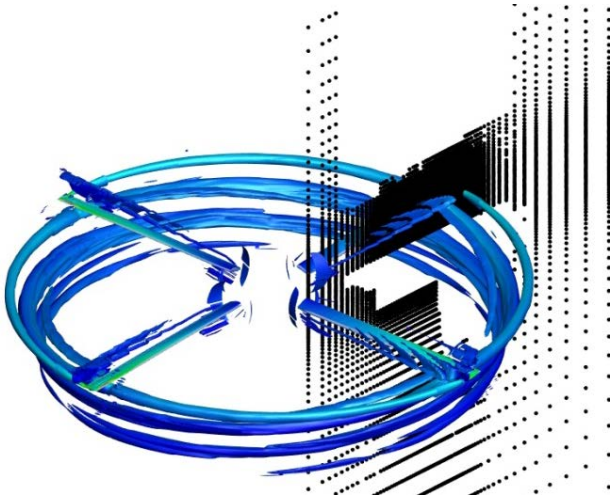

(b) Wavelet (black circle means the cell included in the adaptive dataset)

Fig. 13 Isosurface of Q-criteria, surfaces are colored by Mach contour.

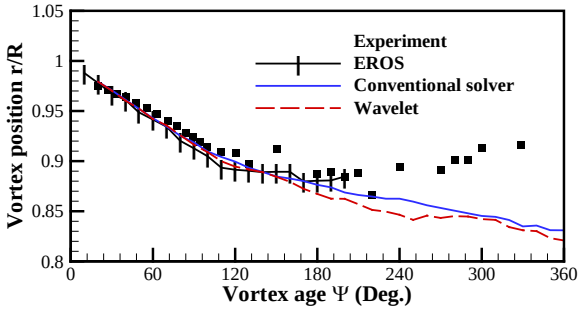

(a) Radial contraction of tip vortex

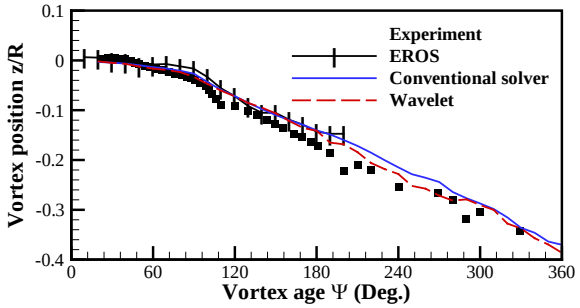

(b) Vertical evolution of tip vortex

Fig. 14 Comparison of tip vortex position

4. CONCLUSION

For the improvement of the computational efficiency in three dimensional helicopter applications, the modified wavelet method was suggested. The high speed and robust calculation is achieved through some modifications: 1) temporal integration (LU-SGS) is conducted only at the cells included in the dataset, 2) the additional cells are selected if this cell are surrounded by the cells included in the dataset, which helps to avoid numerical noise, 3) the decomposition process is executed intermittently. As a result, the modified wavelet method saved 37% of elapsed time on the background grid calculation while the accuracy of solution is mostly preserved. This encouraging improvement proved that the modified wavelet method is useful in hovering rotor applications which the majority of computation domain remains unchanged during the whole computational process. This capability of the wavelet method may be more prominent on larger grid system (the wake regions are relatively decreased) and the forward fight (rotor wakes slide out). However, there are some differences between the conventional solver and the wavelet solver discovered near the wake regions where the abrupt changes of physical properties occur. If the

thresholding criterion is modified to include cells in which the properties are changed rapidly, the accuracy of the adaptive wavelet method may be further improved near the wake regions.

ACKNOWLEGEMENT

This work was supported by the National Research Foundation of Korea (NRF) grant funded by the Korea government (MEST) (No. 2011-0016608).

REFERENCES

[1] Harten, A., “Adaptive Multiresolution Schemes for Shock Computation,” Journal of Computational Physics, Vol. 115, No. 2, pp. 319-338, 1994.

[2] Holmeström, M., “Solving Hyperbolic PDEs Using Interpolation Wavelets,” SIAM Journal on Scientific Computing, Vol. 21, No. 2, pp. 405-420, 1999.

[3] Sjögreen, B., “Numerical Experiments with the Multiresolution Scheme for the Compressible Euler Equations,” Journal of Computational Physics, Vol. 117, No. 2, pp. 251-261, 1995.

[4] Vasilyev, O. V., and Paolucci, S., “A Fast Adaptive Wavelet Collocation Algorithm for Multidimensional PDEs,” Journal of Computational Physics, Vol. 138, No. 1, pp. 16-56, 1997.

[5] Kang, H., Lee, D., and Kim, K., “Improved Computational Efficiency of Unsteady Flow Problems via the Modified Wavelet Method,” AIAA Journal, Vol. 46, No. 5, pp. 1191-1203, 2008.

[6] Park, K., Kang, H., Jeong, J., Lee, D., and Lee, D., “Research on the Adaptive Wavelet Method for the Enhancement of Computational Efficiency of Three Dimensional Flows,” 42nd AIAA Fluid Dynamics Conference and Exhibit, 2012.

[7] Renzoni, P., D’Alascio, A., Kroll, N., Peshkin, D., Hounjet, M. H. L., Boniface, J., Vigevano, L., Allen, C. B., Badcock, K, Mottura, L., Schöll, Kokkalis, A., “EROS – a common European Euler code for the analysis of the helicopter rotor flowfield,” Progress in Aerospace Science, Vol. 36, pp.437-485, 2000.

[8] Srinivasan, G. R., Baeder, J. D., Obayashi, S., and McCroskey, W. J., “Flowfield of a Lifting Rotor in Hover: A Navier–Stokes Simulation,” AIAA Journal, Vol. 30, No. 10, 1992, pp. 2371–2378.

[9] Donoho, D. L., “Interpolating Wavelet Transforms,” Stanford Univ., Dept. of Statistics, TR 408, Stanford, CA, 1992.

APPENDIX. Reference Adaptive Wavelet Method[5] Extended to Three Dimension

The wavelet transformation of this method extends the interpolating subdivision scheme presented by Donoho[9]. It is easy to implement of the existing CFD code, and Kang et al.[5] provided specific criteria of thresholding. The flowchart in Fig. 15 shows the overall implementation of the adaptive wavelet method in the conventional solver. This implementation is composed of the following steps.

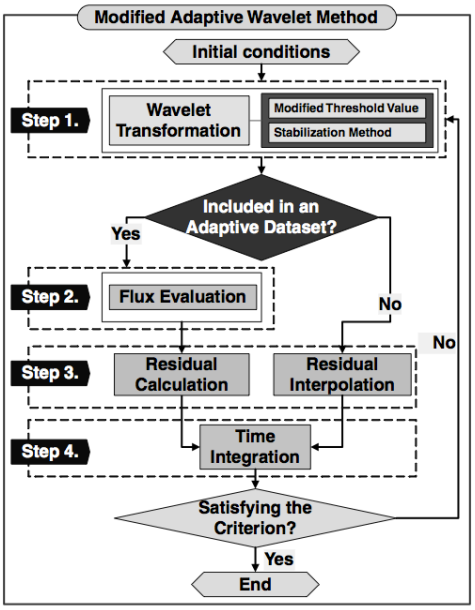

Fig. 15 Overall procedure of flow simulation with the wavelet method.[5]

Step 1. Wavelet Decomposition: To construct the adaptive dataset, decomposition is conducted by interpolating wavelet transformation. Kang et al. [5] described the decomposition by using 6th order interpolating polynomials for two-diemensional applications, and Park et al. [6] extended the adaptive wavelet methods to three-dimension with 4th order interpolating polynomial. In the present work, the three-dimensional decomposition is conducted by 6th order interpolating polynomial for the precise capturing of helicopter vortex.

Assume an initial three-dimensional dyadic grid set in level 1, as shown in Fig. 16. In this figure, ○ cells are compulsory in the adaptive dataset cells and 6th order interpolating polynomial with basis points(○ cells) evaluates values at the other cells as shown in Eq. (3).

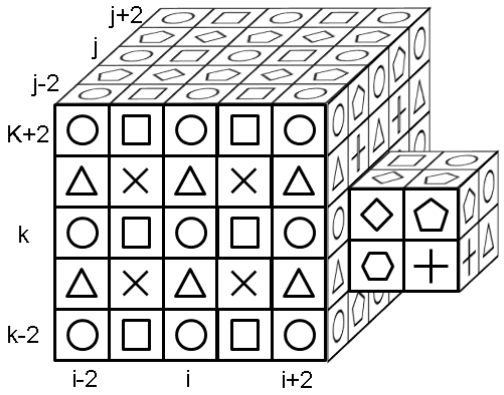

Fig. 16 Three-dimensional dyadic gridset.

(3)

□: $\tilde{Q}^n_{i+1,j,k} = \frac{1}{256}(3Q^n_{i-4,j,k} - 25Q^n_{i-2,j,k} + 150Q^n_{i,j,k}$
$+150Q^n_{i+2,j,k} - 25Q^n_{i+4,j,k} + 3Q^n_{i+6,j,k})$

⬠: $\tilde{Q}^n_{i,j+1,k} = \frac{1}{256}(3Q^n_{i,j-4,k} - 25Q^n_{i,j-2,k} + 150Q^n_{i,j,k}$
$+150Q^n_{i,j+2,k} - 25Q^n_{i,j+4,k} + 3Q^n_{i,j+6,k})$

△: $\tilde{Q}^n_{i,j,k+1} = \frac{1}{256}(3Q^n_{i,j,k-4} - 25Q^n_{i,j,k-2} + 150Q^n_{i,j,k}$
$+150Q^n_{i,j,k+2} - 25Q^n_{i,j,k+4} + 3Q^n_{i,j,k+6})$

◇: $\tilde{Q}^n_{i+1,j+1,k} = \frac{1}{512}(3Q^n_{i-4,j-4,k} - 25Q^n_{i-2,j-2,k}$
$+150Q^n_{i,j,k} + 150Q^n_{i+2,j+2,k} - 25Q^n_{i+4,j+4,k}$
$+3Q^n_{i+6,j+6,k} + 3Q^n_{i-4,j+6,k} - 25Q^n_{i-2,j+4,k}$
$+150Q^n_{i,j+2,k} + 150Q^n_{i+2,j,k} - 25Q^n_{i+4,j-2,k}$
$+3Q^n_{i+6,j-4,k})$

X: $\tilde{Q}^n_{i+1,j,k+1} = \frac{1}{512}(3Q^n_{i-4,j,k-4} - 25Q^n_{i-2,j,k-2}$
$+150Q^n_{i,j,k} + 150Q^n_{i+2,j,k+2} - 25Q^n_{i+4,j,k+4}$
$+3Q^n_{i+6,j,k+6} + 3Q^n_{i-4,j,k+6} - 25Q^n_{i-2,j,k+4}$
$+150Q^n_{i,j,k+2} + 150Q^n_{i+2,j,k} - 25Q^n_{i+4,j,k-2}$
$+3Q^n_{i+6,j,k-4})$

+: $\tilde{Q}^n_{i,j+1,k+1} = \frac{1}{512}(3Q^n_{i,j-4,k-4} - 25Q^n_{i,j-2,k-2}$

$$+150Q^n_{i,j,k} + 150Q^n_{i,j+2,k+2} - 25Q^n_{i,j+4,k+4}$$
$$+3Q^n_{i,j+6,k+6} + 3Q^n_{i,j-4,k+6} - 25Q^n_{i,j-2,k+4}$$
$$+150Q^n_{i,j,k+2} + 150Q^n_{i,j+2,k} - 25Q^n_{i,j+4,k-2}$$
$$+3Q^n_{i,j+6,k-4})$$

$$\hexagon: \tilde{Q}^n_{i+1,j+1,k+1} = \frac{1}{1024}(3Q^n_{i-4,j-4,k-4} - 25Q^n_{i-2,j-2,k-2}$$
$$+150Q^n_{i,j,k} + 150Q^n_{i+2,j+2,k+2} - 25Q^n_{i+4,j+4,k+4}$$
$$+3Q^n_{i+6,j+6,k+6} + 3Q^n_{i-4,j-4,k+6} - 25Q^n_{i-2,j-2,k+4}$$
$$+150Q^n_{i,j,k+2} + 150Q^n_{i+2,j+2,k} - 25Q^n_{i+4,j+4,k-2}$$
$$+3Q^n_{i+6,j+6,k-4} + 3Q^n_{i-4,j+6,k-4} - 25Q^n_{i-2,j+4,k-2}$$
$$+150Q^n_{i,j+2,k} + 150Q^n_{i+2,j,k+2} - 25Q^n_{i+4,j-2,k+4}$$
$$+3Q^n_{i+6,j-4,k+6} + 3Q^n_{i+6,j-4,k-4} - 25Q^n_{i+4,j-2,k-2}$$
$$+150Q^n_{i+2,j,k} + 150Q^n_{i,j+2,k+2} - 25Q^n_{i-2,j+4,k+4}$$
$$+3Q^n_{i-4,j+6,k+6})$$

If the decomposition is executed in higher level, the grid interval of interpolation is set to 2^{level}. In the present work, the multiresolution level of the wavelet is fixed to level 2.

Then the difference between interpolation value and original value can be derived as Eq. (4).

(4)

$$\square: d^n_{i+1,j,k} = Q^n_{i+1,j,k} - \tilde{Q}^n_{i+1,j,k},$$

$$\pentagon: d^n_{i,j+1,k} = Q^n_{i,j+1,k} - \tilde{Q}^n_{i,j+1,k},$$

$$\triangle: d^n_{i,j,k+1} = Q^n_{i,j,k+1} - \tilde{Q}^n_{i,j,k+1},$$

$$\diamondsuit: d^n_{i+1,j+1,k} = Q^n_{i+1,+1j,k} - \tilde{Q}^n_{i+1,j+1,k},$$

$$\mathrm{X}: d^n_{i+1,j,k+1} = Q^n_{i+1,j,k+1} - \tilde{Q}^n_{i+1,j,k+1},$$

$$+: d^n_{i,j+1,k+1} = Q^n_{i,j+1,k+1} - \tilde{Q}^n_{i,j+1,k+1},$$

$$\hexagon: d^n_{i+1,j+1,k+1} = Q^n_{i+1,j+1,k+1} - \tilde{Q}^n_{i+1,j+1,k+1}$$

If the difference is larger than thresholding value ε', the point is included in the adaptive dataset; otherwise, it is excluded from the adaptive dataset.

Park et al.[6] derived the thresholding criterion for three dimension, the thresholding criterion was as same as two dimensional one of Kang et al.[5] as given in Eq. (5).

(5) $$\varepsilon' = min[\varepsilon, \Delta x^m]$$

ε is interpolation error, m means the order of spatial accuracy. In this study, ε is set to 1×10^{-5} and 3rd order MUSCL is used, thus the criterion is applied as Eq. (6).

(6) $$\varepsilon' = min[1 \times 10^{-5}, \Delta x^3].$$

Step 2. Flux Evaluation: After constructing the adaptive dataset, the flag values of the data set determine whether the flux values are to be evaluated or not. If the flag value is 1, the flux value is calculated by Roe's flux-difference splitting method. And MUSCL with 3rd order Koren's limiter is applied to evaluate the flux.

Step 3. Residual Interpolation: On the cell in the adaptive dataset, residual is calculated by using the existing CFD code. Residual on the excluded cell is interpolated in the same way as that of the interpolating wavelet method as Eq. (7).

(7)

$$\square: \tilde{R}^n_{i+1,j,k} = \frac{1}{256}(3R^n_{i-4,j,k} - 25R^n_{i-2,j,k} + 150R^n_{i,j,k}$$
$$+150R^n_{i+2,j,k} - 25R^n_{i+4,j,k} + 3R^n_{i+6,j,k})$$

$$\pentagon: \tilde{R}^n_{i,j+1,k} = \frac{1}{256}(3R^n_{i,j-4,k} - 25R^n_{i,j-2,k} + 150R^n_{i,j,k}$$
$$+150R^n_{i,j+2,k} - 25R^n_{i,j+4,k} + 3R^n_{i,j+6,k})$$

$$\triangle: \tilde{R}^n_{i,j,k+1} = \frac{1}{256}(3R^n_{i,j,k-4} - 25R^n_{i,j,k-2} + 150R^n_{i,j,k}$$
$$+150R^n_{i,j,k+2} - 25R^n_{i,j,k+4} + 3R^n_{i,j,k+6})$$

$$\diamondsuit: R^n_{i+1,j+1,k} = \frac{1}{512}(3R^n_{i-4,j-4,k} - 25R^n_{i-2,j-2,k}$$
$$+150R^n_{i,j,k} + 150R^n_{i+2,j+2,k} - 25R^n_{i+4,j+4,k}$$
$$+3R^n_{i+6,j+6,k} + 3R^n_{i-4,j+6,k} - 25R^n_{i-2,j+4,k}$$
$$+150R^n_{i,j+2,k} + 150R^n_{i+2,j,k} - 25R^n_{i+4,j-2,k}$$
$$+3R^n_{i+6,j-4,k})$$

$$\mathrm{X}: \tilde{R}^n_{i+1,j,k+1} = \frac{1}{512}(3R^n_{i-4,j,k-4} - 25R^n_{i-2,j,k-2}$$
$$+150R^n_{i,j,k} + 150R^n_{i+2,j,k+2} - 25R^n_{i+4,j,k+4}$$

$$+3R^n_{i+6,j,k+6} + 3R^n_{i-4,j,k+6} - 25R^n_{i-2,j,k+4}$$

$$+150R^n_{i,j,k+2} + 150R^n_{i+2,j,k} - 25R^n_{i+4,j,k-2}$$

$$+3R^n_{i+6,j,k-4})$$

+: $\tilde{R}^n_{i,j+1,k+1} = \frac{1}{512}(3R^n_{i,j-4,k-4} - 25R^n_{i,j-2,k-2}$

$$+150R^n_{i,j,k} + 150R^n_{i,j+2,k+2} - 25R^n_{i,j+4,k+4}$$

$$+3R^n_{i,j+6,k+6} + 3R^n_{i,j-4,k+6} - 25R^n_{i,j-2,k+4}$$

$$+150R^n_{i,j,k+2} + 150R^n_{i,j+2,k} - 25R^n_{i,j+4,k-2}$$

$$+3R^n_{i,j+6,k-4})$$

⎔: $\tilde{R}^n_{i+1,j+1,k+1} = \frac{1}{1024}(3R^n_{i-4,j-4,k-4} - 25R^n_{i-2,j-2,k-2}$

$$+150R^n_{i,j,k} + 150R^n_{i+2,j+2,k+2} - 25R^n_{i+4,j+4,k+4}$$

$$+3R^n_{i+6,j+6,k+6} + 3R^n_{i-4,j-4,k+6} - 25R^n_{i-2,j-2,k+4}$$

$$+150R^n_{i,j,k+2} + 150R^n_{i+2,j+2,k} - 25R^n_{i+4,j+4,k-2}$$

$$+3R^n_{i+6,j+6,k-4} + 3R^n_{i-4,j+6,k-4} - 25R^n_{i-2,j+4,k-2}$$

$$+150R^n_{i,j+2,k} + 150R^n_{i+2,j,k+2} - 25R^n_{i+4,j-2,k+4}$$

$$+3R^n_{i+6,j-4,k+6} + 3R^n_{i+6,j-4,k-4} - 25R^n_{i+4,j-2,k-2}$$

$$+150R^n_{i+2,j,k} + 150R^n_{i,j+2,k+2} - 25R^n_{i-2,j+4,k+4}$$

$$+3R^n_{i-4,j+6,k+6})$$

Step 4. Time Integration: After organizing the residual distribution in the whole computational domain, time integration is performed.